Neuron, Vol. 34, 1021–1034, June 13, 2002, Copyright ©2002 by Cell Press

Adaptive Filtering of Vibrissa Input in Motor Cortex of Rat

David Kleinfeld,[1,2,5] Robert N.S. Sachdev,[3,6] Lynne M. Merchant,[1] Murray R. Jarvis,[4,7] and Ford F. Ebner[3]
[1]Department of Physics
[2]Graduate Program in Neurosciences
University of California, San Diego
9500 Gilman Drive 0319
La Jolla, California 92093
[3]Department of Psychology
Vanderbilt University
301 Wilson Hall
Nashville, Tennessee 37240
[4]Division of Biology
California Institute of Technology
Mail Code 219-76
1200 East California Boulevard
Pasadena, California 91125

Summary

We studied the transformation of sensory input as it progresses from vibrissa primary sensor (S1) to motor (M1) cortex. Single-unit activity was obtained from alert adult rats that did not to whisk upon application of punctate, rhythmic stimulation of individual vibrissae. The spike response of units in S1 cortex largely reproduced the shape of the stimulus. In contrast, the spiking output of units in M1 cortex were modulated solely as a sinusoid at the repetition rate of the stimulus for frequencies between 5 and 15 Hz; this range corresponds to that of natural whisking. Thus, the S1 to M1 transformation extracts the fundamental frequency from a spectrally rich stimulus. We discuss our results in terms of a band-pass filter with a center frequency that adapts to the change in stimulation rate.

Introduction

The sensory pathways from the vibrissae to primary somatic sensory (S1) cortex in rodents have been studied intensely as a model sensory system since Woolsey and Van der Loos (1970) first described the topography of the underlying anatomy. Within this system, the location and transient electrical dynamics associated with the vibrissa representation in S1 cortex has been studied repeatedly in anesthetized animals (Ahissar et al., 1997; Armstrong-James and Fox, 1987; Simons, 1978; 1983; Welker, 1971). More recently, the advent of cortical measurements in awake animals (Carvell et al., 1996; Chapin and Lin, 1984; Fee et al., 1997; Nicolelis et al., 1995) has spawned an increasing awareness that the sensory system is of limited value to the animal without the participation of the elaborate motor apparatus that moves the vibrissae into useful positions. In this regard, vibrissa movements are analogous to eye movements (Mays and Sparks, 1980). The vibrissa muscles in the mystacial pad do not exert force against load but, rather, move sensors into a most effective position for probing the environment. Further, the rhythmic motion of vibrissae serves to highlight differences in the nearby tactile space (Carvell and Simons, 1990), much like microsaccades highlight spatial contrast. Thus, behavioral and computational views of vibrissa-mediated somatosensation necessarily include motor, as well as sensory, components that operate in subcortical and cortical loop circuits (Kleinfeld et al., 1999).

Anatomical studies have identified strong and topographically reciprocal connections between vibrissa-related primary motor (M1) and S1 cortices (Izraeli and Porter, 1995; Keller et al., 1996; Kim and Ebner, 1999), as well as subcortical thalamic afferents that arise from the vibrissa areas of the ventral lateral (VL) thalamic nucleus or the medial division of the posterior (PoM) thalamic nucleus. The latency of sensory-evoked responses in rat M1 cortex is several milliseconds longer than the latency in S1 cortex (Farkas et al., 1999) or PoM thalamus (Diamond et al., 1992; Chiaia et al., 1991; Sosnik et al., 2001). While this implies that efferents from either S1 cortex or PoM thalamus may generate the initial response in vibrissa M1 cortex, the amplitude of the stimulus-evoked response in M1 cortex was essentially extinguished after either lidocaine application to S1 cortex to block action potentials or the ablation of S1 cortex (Farkas et al., 1999). In an analogous case, significant reductions in M1 cortical responses were found after lesions to S1 cortex in cat (Andersson, 1995; Herman et al., 1985) and in Macaca monkey (Asanuma et al., 1980). Thus, an important observation about sensory responses in vibrissa M1 cortex of the rat is that they depend almost completely upon input from S1 cortex.

Here, we report on the sensory-evoked response in the vibrissa subdivision of primary motor (M1) cortex. We asked several questions. (1) What features of the sensory-induced movement of the vibrissae are represented by spike trains in M1 cortex? In particular, the results of past studies suggest that units in vibrissa M1 cortex may encode only slow movements of the vibrissae (Carvell et al., 1996; Swadlow, 1994). (2) Are the potential features compatible with a linear response mechanism as it applies to unit responses in S1 cortex (Fee et al., 1997), or do they make use of a nonlinear or adaptive mechanism?

Our preparation consisted of awake animals that were trained to maintain the position of their vibrissae in the presence of periodic deflections of a vibrissa with a localized air puff. We recorded single-unit activity and analyzed the responses in the frequency domain, where statistical techniques provide a means to estimate confidence intervals for features of the response. The activity in vibrissa M1 cortex was contrasted with that recorded simultaneously from S1 cortex.

[5]Correspondence: dk@physics.ucsd.edu
[6]Present address: Division of Life Sciences, Cajal Research Center, University of Texas-San Antonio, San Antonio, Texas 78249.
[7]Present address: Technology Sources Ltd., 2 Signet Court, Swanns Road, Cambridge CB5 8LA, United Kingdom.

Results

Location of Recording Sites

There is some discord as to the exact location and continuity of M1 vibrissa cortex (Donoghue and Sanes, 1988; Donoghue et al., 1990; Donoghue and Wise, 1982; Gioanni and Lamarche, 1985; Izraeli and Porter, 1995; Jacobs and Donahue, 1994; Miyashita et al., 1994; Neafsey et al., 1986; Sanderson et al., 1984; Sharp and Evans, 1982; Weiss and Keller, 1994). Thus, we used standard stimulation procedures (see Experimental Procedures) and derived maps for our species and age group of rats. We found that there is a contiguous region in frontal cortex for which microstimulation with peak amplitudes of 20 to 40 μA led to motion of the vibrissae (low-threshold area in Figure 1A). The location of this region is consistent with that described previously for rat. In addition, we observed a separate region in the parietal cortex for which microstimulation with peak amplitudes of 40 to 60 μA led to motion of the vibrissae (high-threshold area in Figure 1A). This region spans the primary vibrissa and dysgranular areas of somatosensory cortex and is in accord with the findings of Gioanni and Lamarche (1985). We chose to place our recording chamber for M1 cortex over the low-threshold area of frontal cortex (Experimental Procedures). The recording chamber for S1 cortex was placed over parietal cortex using previously defined coordinates (Experimental Procedures).

At the termination of each recording session, we reconstructed the tracks of selected electrodes to confirm that they remained in the specified regions of cortex (Experimental Procedures; Figures 1B and 1C). For the example of Figure 1C, the lesion that marks the end of the electrode (arrow) is close to the medial edge of the barrel field and is consistent with the finding that the principal vibrissa for this electrode was E1. Here, as in general, the majority of the electrodes were located in the vicinity of the layer 4 to 5 border.

Stimulation Paradigm

We stimulated individual vibrissae with a localized pulse of air to achieve a maximum deflection amplitude of 5° (Figure 2A; Experimental Procedures). Our stimuli were confined only to the major vibrissae, i.e., the straddlers and those in the posterior three arcs of rows (B), (C), or (D) in Figure 2. The onset time and shape of the pulse were observed via the output of a piezoelectric transducer. The rise and fall times of the pulse were 2 to 4 ms, and the duration at full-width half-maximal amplitude was 20 ms (Figure 2B).

We used exaggerated deflections of 17°, over three times the normal deflection of 5°, to examine the timing of the vibrissa motion and check for the potential activation of neighboring vibrissae. We observed that the deflections occur over a period of 4 ms, concomitant with the onset of the air puff; (t = 28 and 32 ms frames in Figure 2A). We also observed no discernable motion of neighboring vibrissae or contact between vibrissae (Figure 2A), even for this highly exaggerated deflection. Movement of a single vibrissa, rather than multiple vibrissae, minimizes the interaction among neurons in S1 cortex (Simons, 1983; 1985) and thus simplifies the sensory input.

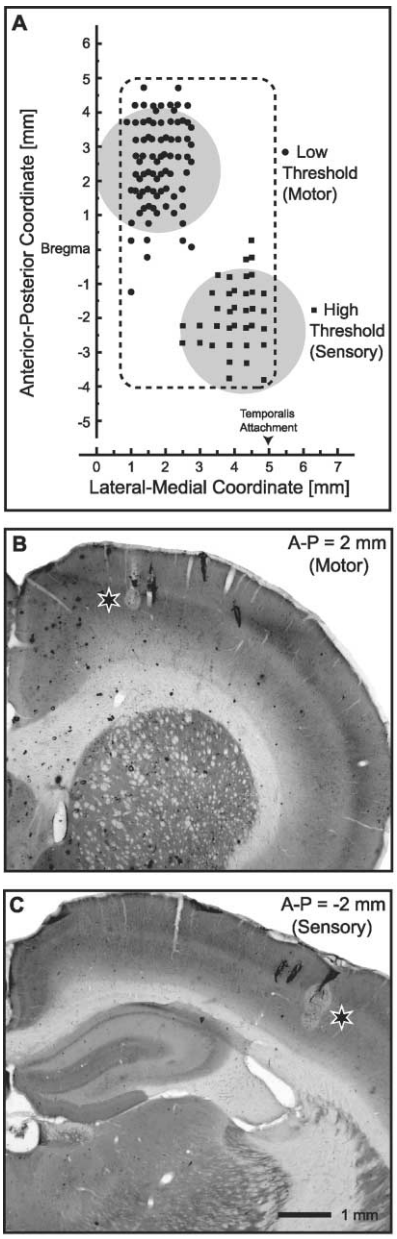

Figure 1. Identification of Recording Sites

(A) Maps of vibrissa movement in response to electrical microstimulation in frontal and parietal cortex are shown. Sites throughout the entire field were stimulated (Experimental Procedures). Those marked with symbols elicited small movements of the vibrissa. The low-threshold region is associated with primary vibrissa motor (M1) cortex, and the high-threshold region overlaps primary sensory (S1) cortex and is likely to encompass the medial edge aspect of vibrissa S1 cortex as well as the dysgranular zone.

(B and C) Coronal sections stained for cytochrome–*c* oxidase taken from M1 and S1 cortices, respectively, are shown. The electrolytic burn marks, labeled with a closed star symbol (⋆), indicate the location of recording electrodes in M1 and S1 cortices.

Control for Reflexive Movements

Our experimental paradigm assumes that the animals hold their vibrissa fixed, so that neurological signals in M1 cortex can be related to the stimulus input and not to motor output. We thus checked if periodic deflection of the vibrissae led to a reflexive entrainment of vibrissa

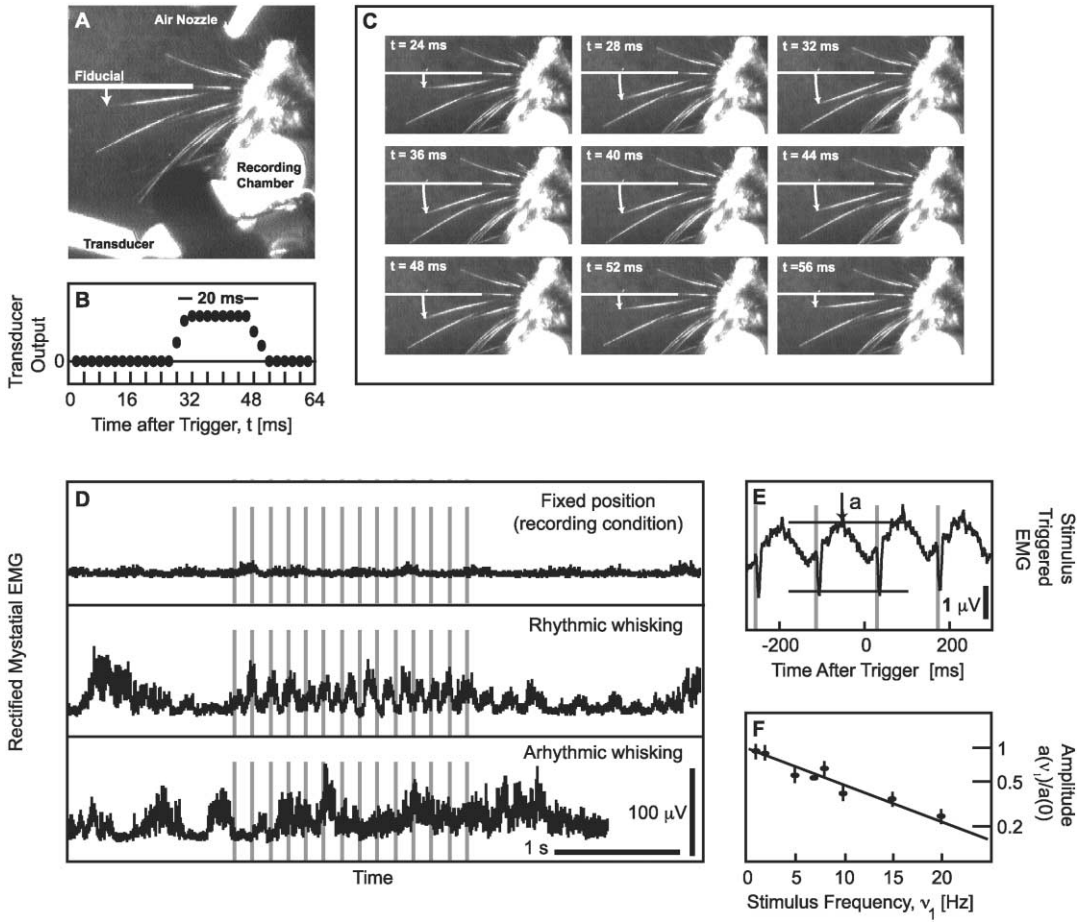

Figure 2. Characterization of the Air Puff Stimulus and the Reflexive Response of the Mystacial Pad to the Stimulus

(A) An overview of the preparation is depicted. An air nozzle that directed a localized puff of air is shown aimed at vibrissa C1. The transducer is a piezoelectric film that is deflected by the puff. The head of the animal is fixed in place and the body is supported by a tube. The chamber over M1 cortex is shown sealed with a cap. The fiducial line and arrow are drawn solely to indicate the position of the C1 vibrissa.

(B) Here, the output from the piezoelectric transducer is plotted as a function of time. The delay from the time of the electronic trigger to the onset of the puff was 20 ms. Note that the onset of this transducer signal is coincident with the onset of vibrissa deflection.

(C) A sequence of frames, acquired every 4 ms, shows the position of the vibrissa versus time. Note the onset of deflection of C1 in the caudal direction at $t = 24$ ms and the recovery of the initial position at $t = 48$ ms. The whisker remained passively deflected throughout the stimulus.

(D) Rectified EMG activity during three epochs of continuous stimulation (gray lines) at 7 Hz are shown. Epoch 1 has only a constant, low level of activity and is typical of the conditions during recording of unit activity. Epochs 2 and 3 show EMG activity at times when the rat was induced to move its vibrissae. Note that the activity, even for the case of rhythmic whisking (epoch 2), is obviously not entrained to the 7 Hz stimulation frequency.

(E) The stimulus-averaged EMG activity for stimulation at 7 Hz is depicted. We averaged 200 s of data (1400 stimuli). Note that rapid retraction follows the puff. The amplitude of this signal is about 0.03 times that seen during active whisking (epoch 2 in [D]).

(F) The normalized peak-to-peak amplitude of the stimulus entrained component of the EMG as a function of stimulation frequency is plotted. The data for each of the five animals was normalized to the response at 7 Hz. Note the exponential falloff in amplitude with increasing frequency.

movement. The rectified mystacial electromyogram (EMG) was recorded during epochs of spontaneous activity, as well as during stimulation (Experimental Procedures). In general, the EMG activity was relatively low as the rat held its vibrissae at constant position. No aspect of the EMG activity appeared to follow the stimulus (segment 1 in Figure 2D). Further, the rat could be induced to whisk (segment 2 in Figure 2D) or protract and probe with its vibrissae (segment 3 in Figure 2D) for selected epochs. In all cases, even in the presence of rhythmic whisking, there was no obvious synchrony between the EMG output and the rhythmic stimulus.

As a means to quantify a potential low level of entrainment, we correlated the EMG activity with stimulation for periods of 100 s. For a particular data set with a stimulus repetition rate of 7 Hz (Figure 2E), we observed that the stimulus-triggered EMG had an amplitude that was less than 0.03 times that of the EMG associated with natural whisking (cf. segment 2 in Figure 2D with Figure 2E). Qualitatively similar results were observed with all other animals ($n = 5$). This result shows that the reflexive response is weak, albeit not zero. Lastly, the amplitude of the reflexive response is seen to decrease with increasing stimulation frequency (Figure 2F).

Unit Recordings

We focus first on a specific example to illustrate the typical response for units in S1 and M1 cortices

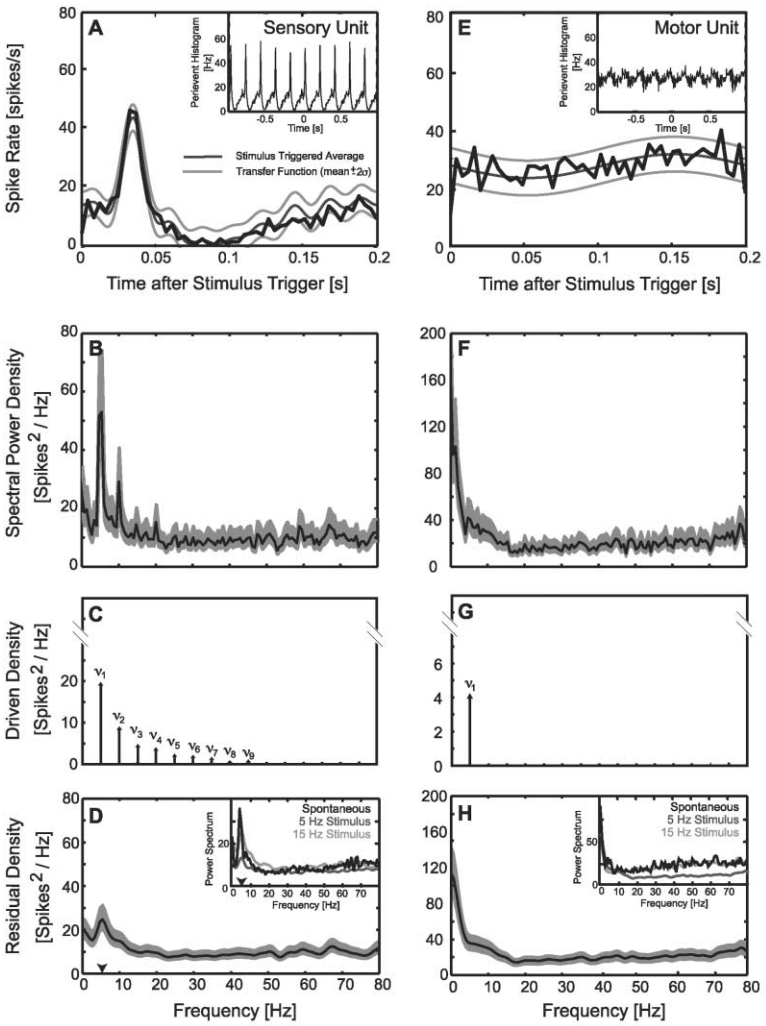

Figure 3. The Nature of the Response for Units in S1 (Left Column) versus M1 (Right Column) Cortex and Their Spectral Decomposition

(A and E) The stimulus-triggered average (thick black line and insert) and the transfer function between the stimulus and the instantaneous spike rate of sensory and motor units (thin black line) for vibrissa stimulation at 5 Hz are plotted. The transfer function was computed from a spectral decomposition of the entire 100 s time series of the response. The 95% confidence (approximately 2 SD) limit for the transfer function is indicated by the thin, gray lines. Note the punctate response for the case of a unit from S1 cortex, along with the delayed underlying response, and the broad response for the unit from M1 cortex.

(B and F) The spectral power density of the entire time series of the unit spike response, along with the 95% confidence limits on the spectral density are plotted. The spectral estimator had a bandwidth of 1.0 Hz.

(C and G) The spectral power density for the stimulus-driven part of the response is depicted. The height of each arrow corresponds to the magnitude of the coefficient for power at the fundamental frequency of the periodic stimulus, denoted ν_1, or at the n-*th* harmonic of the stimulus, denoted ν_n, where $\nu_n = n \times \nu_1$. Only coefficients that surpassed the value set by an F test at the 95% confidence level were accepted. Note that the stimulus-driven spectrum for the sensory unit has multiple harmonics, consistent with a pulsatile response, while that for the motor unit has power only as the fundamental frequency (i.e., the stimulus repetition rate). These coefficients, along with their phase, were used to reconstruct the transfer functions shown in parts (A) and (E), respectively.

(D and H) The spectral power density for the residual response. This density was found by subtracting the stimulus driven components in the spectral power density ([C] and [G]) from the spectrum for the entire spike train ([B] and [F]). For the case of the sensory unit, note the excess power near 5 Hz (arrowhead in [D]), which lies close to the driven frequency in this example. To demonstrate that this residual response represents background activity of the unit rather than an unforeseen deficit in our numerical analysis, we show that the spectral power density for a 100 s epoch of spontaneous activity taken immediately before the stimulus was applied together with the residual response for stimulation at 5 and 15 Hz (insert in [D]). Note the peak at 5 Hz (arrowhead in insert in [D]) in the data for spontaneous activity as well as residual activity in the sensory unit. This demonstrates that the spiking output of the driven unit was phase-locked to a 5 Hz stimulus, as well as being spontaneously active near 5 Hz; the latter activity was incommensurate with the stimulation. Lastly, note the presence of low-frequency spiking in the residual activity for the motor unit as well as in the spontaneous activity for the same unit (insert in [H]).

(Figure 3). The stimulus was a 5 Hz repetitive air puff to whisker D2. We calculated the event-triggered average to form the instantaneous spike rate as a function of time over one period of the stimulus (100 s for a total of 500 events) (inserts in Figures 3A and 3E).

The Basic Response in S1 Cortex

We observed that the unit in S1 cortex had a rapid initial response (Figure 3A) so that the stimulus-triggered average spike train appeared as a sequence of pulses (insert to Figure 3A) that approximated the form of the stimulus (Figure 2C). The width of the initial response was 16 ms, and the latency to the peak of the response relative to the onset of the puff was approximately 10 ms. The width is somewhat greater than that published for anesthetized animals (Armstrong-James et al., 1992), as would be expected, with slight changes in the position of the vibrissae over the course of a measurement. In addition to the punctate, initial response, there was a broad, long-latency response (Figure 3A). This component has also been observed in anesthetized animals (Armstrong-James and George, 1988; Chapin et al., 1981; Kleinfeld and Delaney, 1996), although it is known to be labile for measurements performed under anesthesia (Chapin et al., 1981).

The Basic Response in M1 Cortex

In contrast to the result for S1 cortex (Figure 3A), the spiking output of the unit in M1 cortex exhibited only a smoothly varying response across the entire interstimulus interval (Figure 3E). Thus, the response for this unit appears as a weak sinusoidal modulation of a spike rate (insert in Figure 3E), as opposed to the set of periodic pulses that formed the stimulus. Further, the maximum modulation of the spike rate was relatively weak compared with that of the sensory unit. The maximum

change in rate was about 15% of the baseline rate for this unit.

Spectral Decomposition of the Unit Response

As a means to arrive at an unbiased measure of the spike response, particularly the relatively broad and weakly modulated responses for units in M1 cortex, we decomposed each measured response into stimulus driven components and a residual component (Experimental Procedures; Equation 1). The spectral power density for the driven part, denoted $\tilde{S}_{driven}(\nu)$, is defined in terms of sinusoids at the fundamental frequency of the stimulus, ν_1, and at harmonics of the fundamental frequency that are locked to the repetition rate of the stimulus (Equation 2). We retained only components that were significant at the 95% confidence level. These coefficients were further used to construct the transfer function (Equation 3). The spectral density of the residual component of spike trains, denoted as $\tilde{S}_{residual}(\nu)$ (Equation 1), represents background spike activity that is not locked to the stimulus.

For illustration, we again consider the data of Figure 3 with a drive frequency of $\nu_1 = 5$ Hz. For the sensory unit, the spectral power density shows a smoothly varying baseline and a clear series of peaks near 5, 10, 15, and 20 Hz (Figure 3B). The driven part of the spectral density was found to consist of statistically significant peaks at the fundamental frequency, ν_1, and the first eight harmonics of the drive frequency, i.e., ν_1 through $\nu_9 = 9 \times \nu_1$ (Figure 3C). The transfer function that was reconstructed from this spectral decomposition, which is statistically equivalent to the stimulus-triggered average, was seen to fit the calculated average to well within the 95% confidence limits (thin lines in Figure 3A).

The residual spectral density for this example, $\tilde{S}_{residual}(\nu)$, exhibited a smoothly varying baseline and a broad peak near 5 Hz (Figure 3D). Although this center frequency is close to that of the stimulus, a residual peak can, in principle, occur as a result of an intrinsic neuronal oscillation that is incoherent with the stimulus. As a control to check that this peak was not the result of an unaccounted systematic error in our spectral estimation procedures, we calculated the spectral power density for an equivalent interval of time immediately before stimulation. We again obtain the peak centered at 5 Hz (insert in Figure 3D), which verifies the fidelity of our spectral estimation procedures. Further, a similar peak is seen in the residual spectrum when the drive frequency was 15 Hz rather than 5 Hz (insert in Figure 3D).

The spectral power density of the spike train of the motor cortical unit exhibited a broad peak at low frequencies but was otherwise featureless (Figure 3F). This spectrum was found to consist of a statistically significant peak only at the fundamental frequency (Figure 3G). The transfer function thus consists of a background rate that was modulated purely as a sinusoid. This function and the associated 95% confidence intervals are seen to fit the stimulus-triggered average quite well (thin lines in Figure 3E). Lastly, the residual spectrum for this example exhibited a smoothly varying baseline and a broad peak near zero frequency (Figure 3G). As in the case of the sensory unit, this motor unit shows a similar spectral peak in its spontaneous activity prior to the stimulus epoch (insert in Figure 3G).

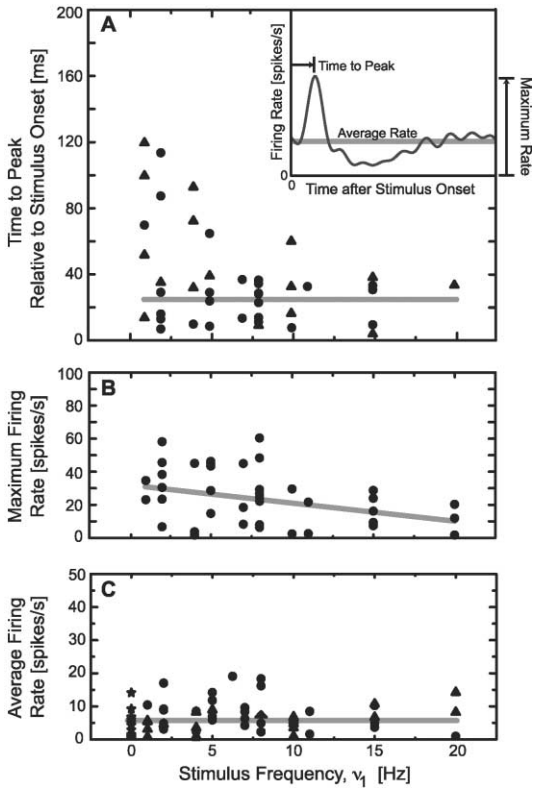

Figure 4. Summary of the Properties for All Vibrissa S1 Cortical Units in Our Data Set

Those measured coincident with a motor unit that showed only a response at the stimulation frequency, ν_1, are indicated with a closed circle and the remainder with a closed triangle.

(A) The time from the onset of the air puff to the peak of the initial, punctate response is plotted. The gray line through the data points corresponds to a latency of 25 ms. The insert shows the definition of this measure, as well as those used in (B) and (C).

(B) The maximum spiking rate for all units is shown. The gray line is from a linear fit to the data, with the rate being equal to 32 s^{-1} − 1.09 × f, and shows that there is a trend for the peak rate to decrease with increasing stimulation frequency.

(C) The average spiking rate for all units is shown. The data for the stimulation frequency $\nu_1 = 0$ corresponds to spontaneous activity. The gray line corresponds to the average rate, which is independent of the stimulation.

Punctate Responses for Units in S1 Cortex

The response of all of the units from S1 cortex were locked to the stimulus. The vast majority of units, i.e., 83% (43 out of 52), exhibited a punctate response for the full range of stimulation frequencies used in this study (1 to 20 Hz). Approximately one third of these units (15 out of 43) further exhibited a discernable delayed response, as in figure 3A. The remaining 17% (9 out of 52) of the responses corresponded to a sinusoidal modulation of the spike rate that was similar to that of the typical motor units (Figure 3E).

The temporal aspects of the response of all units in S1 cortex were summarized in terms of a set of parameters (insert in Figure 4A). The latency to the peak of the initial response was quite variable for low stimulation frequencies (i.e., less than 5 Hz) and then approached a plateau value of about 25 ms (Figure 4A). The magni-

tude of the peak of the initial response also decreased as a function of stimulation frequency (Figure 4B). These results are consistent with those in studies on the spike response of units in a mixture of layer 4 and layer 5 neurons (Simons, 1978; Ahissar et al. 2000). Units in layer 4 nominally exhibit a constant latency while those in layer 5 exhibit a latency that decreases with increasing stimulation rate. Lastly, the spike rate of our units from S1 cortex were essentially independent of the stimulation frequency (Figure 4C). On average, the rate was 5.6 $\pm$ 4.4 Hz (mean $\pm$ SD), and the spontaneous rate was essentially the same as the driven rates (Figure 4B). In toto, the correspondence between the essential results with our awake preparation and past results with paralyzed or anesthetized animals validate our preparation as a behavioral model.

Adaptive Tuning for Units in M1 Cortex

The spiking output of approximately one third of the units in M1 cortex was phase locked to the stimulus (75 of 195 records). Of these, 85% (63 of 75) responded solely at the stimulus frequency, ν_1, for the full range of 1 to 20 Hz stimulus repetition rates. This is illustrated for a specific unit (insert to Figure 5A) that responded with sinusoidal modulation of its spiking output for stimulation at either 4 Hz (Figure 5A), 7 Hz (Figure 5B), 10 Hz (Figure 5C), or 15 Hz (Figure 5D). At each stimulation frequency, only the spectral component at ν_1 was statistically significant.

The response for all records was parameterized by the fraction of power in the driven response that was at the stimulus frequency, denoted $\delta S_{driven}(\nu_1)$ (Equation 4). We observed that this fraction was $\delta S_{driven}(\nu_1) = 1$ over the range 5 Hz $< \nu_1 <$ 15 Hz (Figure 5E); this frequency range corresponds to the band over which animals whisk (O'Connor et al., 2002). Outside of this frequency range, a sizable fraction of the responses (38%) contained harmonics at the stimulus frequency so that their spiking outputs were not modulated as pure sinusoids.

Unlike the temporally sharp response for units in S1 cortex where a measure such as latency is appropriate, the responses for units in M1 cortex were spectrally sharp so that appropriate measures are the relative amplitude and phase of the sinusoid (insert in Figure 6A). We define the relative modulation, denoted A_1, as the absolute modulation amplitude relative to the background level, with $0 \leq A_1 \leq 1$ (Equation 5). We further define the phase relative to a value of 0 radians at the trigger to the stimulus (Equation 5). The relative amplitude of the modulation was variable at low stimulation frequencies but, on average, a constant across all frequencies with $|A_1| = 0.12 \pm 0.05$ (mean $\pm$ SD) (Figure 6A). The responses were uniformly distributed as a function of phase (Figure 6B). Lastly, the firing rate of units in M1 cortex was variable at low stimulation frequencies (i.e., less than 5 Hz) but then approached a constant value (Figure 6C). On average, the rate was 7.0 $\pm$ 7.0 Hz (mean $\pm$ SD).

In toto, the essential aspect of this data is that the form of the temporal response remains a pure sinusoid as the repetition rate of the stimulus is varied by a factor of three. This result is particularly robust in that it encompasses the natural whisking frequencies (gray band in Figure 5E). Further, different units have different preferred phases. This distribution is similar to the distribution of preferred phases for units in S1 cortex during active whisking in air (Fee et al., 1997).

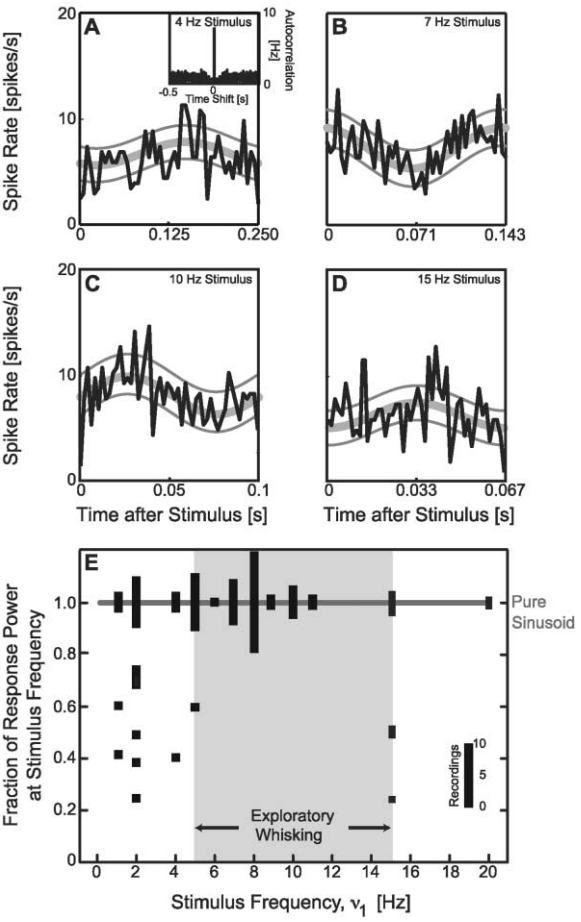

Figure 5. Summary of the Sinusoidal-like Response of Units from Motor Cortex to Punctate Stimuli

(A–D) Results from a particular unit that show the peristimulus time histogram (black curve) and the best fit (gray curve) at three different stimulation frequencies (i.e., 4, 7, 10, and 15 Hz). Note that at all four frequencies, the spiking output of the unit is essentially modulated as a sinusoid (i.e., the modulated rate captures only the fundamental frequency of the repetitive stimulus for the criteria of a 95% confidence interval on each spectral component (see Figure 3G). The insert in (A) shows the autocorrelation for the unit over all stimulation conditions; note the relative refractory period below time shifts of $\sim$100 ms. The absence of spikes near a time shift of zero is evidence that this is a single unit.

(E) Summary of the relative power in the fundamental mode, $\delta S_{residual}(\nu_1)$ (Equation 4), for all motor units in this study is depicted. A value of one for this fraction indicates that the unit extracts only the fundamental frequency of the stimulus (i.e., the response is a pure sinusoid whose frequency is the repetition rate of the stimulus). The vertical extent of a bar corresponds to the number of data points (i.e., 16 separate units at 8 Hz).

Background Oscillations for Units

In light of the partial entrainment of many units in M1 cortex to the stimulation frequency (Figure 3H), we examined the tendency of units to produce oscillatory spiking (i.e., excess spiking in a narrow frequency band) during periods of spontaneous activity. Three classes emerged. A first class encompassed units with a statistically significant tendency to spike in a band between 5

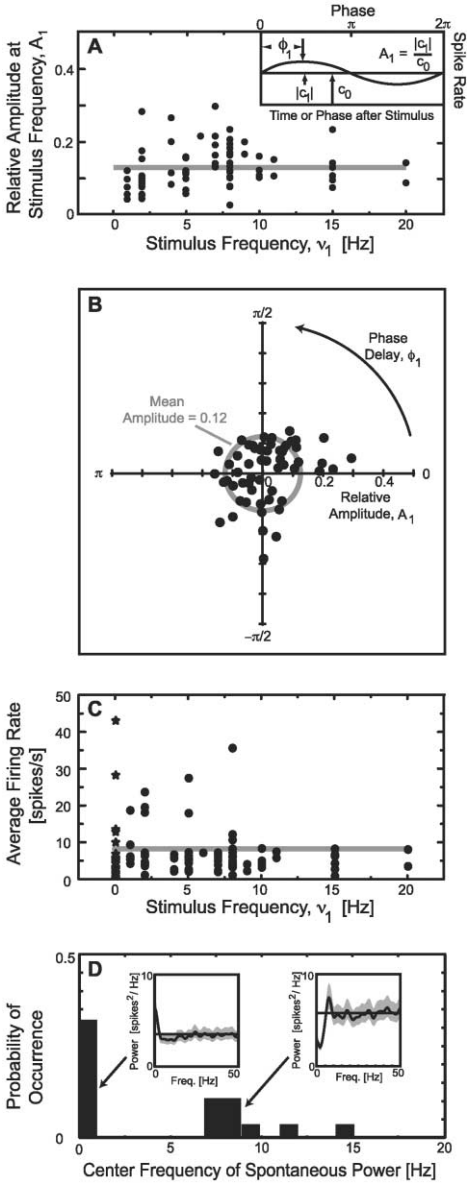

Figure 6. Summary of the Properties of All Motor Responses in Our Data Set that Showed a Response at the Stimulus Frequency

(A) The relative magnitude of the modulation depth, A_1 (Equation 5), for units whose spiking was modulated only at the fundamental frequency of the stimulus is shown. The gray line corresponds to the average value and is independent of the stimulation frequency at the 95% confidence level. The insert illustrates the definition of the measured quantities.

(B) The relative magnitude of the modulation depth and phase delay (Equations 5 and 6) is shown for units whose spiking was modulated only at the fundamental frequency of the stimulus. The data for all stimulus frequencies were pooled. Note that there is no preferential phase.

(C) Here, the average spiking rate for all units is shown. The data for the stimulation frequency of zero corresponds to spontaneous activity. The straight gray line corresponds to the average rate of 7.0 Hz.

(D) The histogram of the spectral power density of the spontaneous spike activity for all motor units that exhibited a significant spectral peak is depicted. The inserts show the full spectra for two particular units. The left-side insert shows a unit whose spiking output showed a significant tendency to periodically spike near 7 Hz (indicated by a closed star symbol); the significance is established by the deviation of the 95% confidence interval from the mean rate. The right-side insert shows a unit whose spiking output showed a significant tendency to produce excess spikes at low frequencies, with a peak below the resolution of 1 Hz (closed star symbol). The best estimate (100 s time series, 1.0 Hz bandwidth) is depicted as the thick line, the 95% confidence limits are shown in gray, and the mean rate is depicted as a thin line.

and 9 Hz (29% or 8 of 28 units across five animals; Figure 6D and right-hand insert in the Figure); significance was judged by a spectral peak that exceeded the mean rate at the 95% confidence limit (gray bands in inserts to Figure 6D). A second class encompassed units with a significant tendency to produce a low-frequency rhythm that peaks below 1 Hz frequency (31%; Figure 6D and left-hand insert in the Figure). A third class encompassed units with featureless spectral densities (40%). These data suggest that M1 cortex contains units that can function as intrinsic oscillators. Further, during epochs of stimulation, all of these units were partially entrained to the stimulus frequency.

In contrast to the results for vibrissa M1 cortex, the spontaneous activity from only a single unit from S1 cortex data showed a statistically significant tendency to spike in a band that was centered away from zero frequency (1 of 16; Figure 3D). This suggests that sustained spontaneous oscillations in S1 cortex are less pronounced in awake animals than in the anesthetized rat (Ahissar et al., 1997). We did observe a strong tendency for units in S1 cortex to produce excess spikes below 1 Hz (50%; data not shown), qualitatively consistent with the findings for anesthetized animals (Ahissar et al., 1997).

Discussion

The central finding of this study is that units in vibrissae M1 cortex transform the punctate vibrissa deflections into a sinusoidal response (Figures 3E–3G, 5, and 6). The stimulus-evoked spikes for units in S1 cortex mimic the temporal form of the sensory stimulus as the firing rate captures both the fundamental and harmonic frequencies that comprise the mathematical description of the temporal patterns of the applied stimuli (Figures 3A–3C). The spike rate for units in M1 cortex carry forward only the fundamental frequencies for stimuli applied at different frequencies; however, the harmonic frequencies are not encoded in unit activity recorded from M1 cortex (Figures 3 and 5). This transformation occurs over a broad range of stimulus frequencies, 5 to 15 Hz (Figure 5E), which corresponds to the range of contacts predicted to occur during natural whisking (Figure 5E). To model this transformation, a mechanism is required that allows motor cortex to adapt to different fundamental frequencies while remaining unresponsive to the substantial harmonic activity that occurs in S1 cortex. This computation is similar to that necessary for the identification of pitch in audition (Hess, 1982; Pierce, 1991).

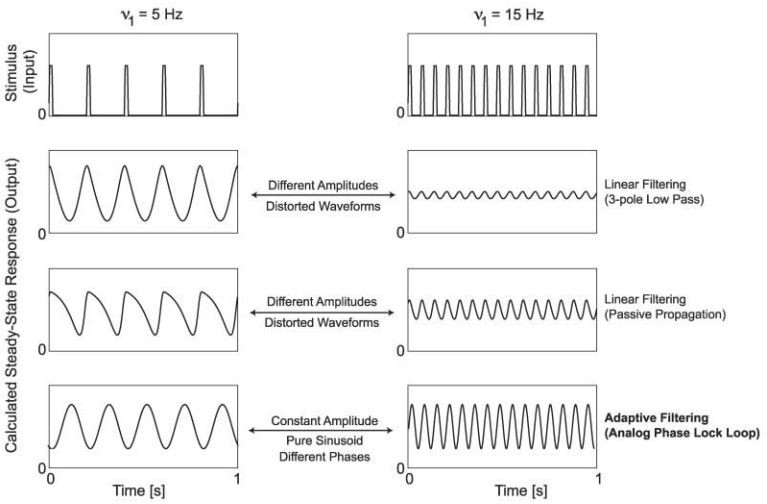

Figure 7. Comparison of Passive versus Adaptive Filtering of a Time Series of Pulses

Time series of pulse stimuli with identical widths but with repetition rates of $\nu_1 = 5$ and 15 Hz, respectively, for the left and right columns (top row) are shown. The two stimulus time series convoluted with a three-pole low-pass linear filter (Equation 7, with $\tau = 32$ ms and $n = 3$), are shown in the second row. In the third row, the two stimulus time series are shown, convoluted with the dispersion for passive propagation along a linear cable (Equation 8, with $\tau = 32$ ms and $X = 2$). In the bottom row, the two stimulus time series are depicted after passing through an analog phase-locked loop (Equation 10, with $n = 1$, $f(x) = x$, $\nu_0 = 7$ Hz, and $g\,|a_1| = 40$ Hz).

Neuronal Mechanisms for the Computation of the Fundamental Frequency

The work of Toldi and coworkers (Farkas et al., 1999) strongly suggests that the input to vibrissa M1 cortex is dominated by efferents from S1 cortex. We argue that the sinusoidal response in vibrissa M1 cortex is incompatible with a linearly filtered version of the pulsatile response in S1 cortex. However, an adaptive filter, i.e., one with a narrow pass-band whose center frequency changes in response to a change in the input, provides a means to extract only the fundamental component from the broadband pulsatile signal in S1 cortex.

Linear Filters

Recall that the spike rate in M1 cortex is modulated only at the fundamental frequency of the stimulation for punctate inputs at a 5 Hz repetition rate. Thus, the harmonics at 10 and 15 Hz are suppressed. Yet the observed responses for stimulation frequencies of 10 and 15 Hz and higher (Figure 5C) have an amplitude that is as large as the response at 5 Hz (Figure 6A) The lack of a consistent attenuation with increasing frequency points to the failure of linear filtering.

To be concrete, we illustrate the difficulty with linear filters by considering the response for trains of 5 versus 15 Hz pulsatile inputs (top row in Figure 7) with two specific realizations. The first example involves a three-pole low-pass filter (Equation 7), as could occur with a feedforward path through three levels of neurons. In order to achieve filtering that resembles a sinusoid at 5 Hz, albeit with noticeable distortion and thus power at the harmonics of the stimulation frequency, we incur a substantial reduction in amplitude at 15 Hz (second row in Figure 7). A single-pole filter would have less attenuation at 15 Hz but would add considerably more distortion to the waveform at 5 Hz. The second example is a linear transmission line with a length equal to two electronic distances (Equation 8), as could occur for passive propagation in a dendrite. The trade-off between distortion in the waveform for the 5 Hz stimulation and the decrement in amplitude for the 15 Hz stimulation is worse than for the low-pass filter (third row in Figure 7).

Coupled Oscillators as Adaptor Filters

Phase locking occurs between neuronal oscillators that are coupled only weakly (Equation 9) in the sense that the oscillators affect the timing of each other's output, but not the shape of their respective action potentials (Ermentrout and Kleinfeld, 2001). This provides a means to lock the output of motor and sensory cortical units over a range of frequencies (Sompolinsky et al., 1990), which is 1 to 20 Hz in the present case (Figure 5E). While not impossible, there is presently no apparent mechanism for a circuit of coupled oscillators to phase lock at solely the fundamental frequency for a subset of these frequencies, 5 to 15 Hz in the present case (Figure 5E). Thus, the predicted behavior for pairs or networks of weakly coupled oscillators appears to be in disagreement with the observed response for neurons in M1 cortex.

Phase-Locked Loops as Adaptor Filters

A general form of an adaptive filter is the analog phase-locked loop (PLL) (Best, 1984). The analog PLL contains three essential components (see Experimental Procedures). (1) The mixer that combines two different inputs, as may occur by forming their products (inputs R(t) and O(t) and output M(t) in Figure 8A). The output of the mixer contains a constant term, as well as periodically varying terms, when the two inputs have the same frequency. (2) The controlled oscillator has a frequency that is shifted from a baseline value to a frequency above or below the baseline by a control signal (output O(t) and control input C(t) in Figure 8A). (3) The low-pass filter attenuates the periodic factors in M(t) so that the steady-state phase difference between R(t) and O(t) may be used to control the oscillator (inputs M(t) and output C(t) in Figure 8A). These three components form a closed-loop circuit in which the frequency of an incoming periodic signal is expressed in terms of a control signal whose amplitude or phase, depending on the detailed realization, is proportional to the incoming frequency (Equation 10). The control signal drives the oscillator so that it can track the fundamental frequency of the reference.

The calculated response of the controlled oscillator in an analog PLL is qualitatively consistent with the form of the responses observed in M1 cortex (bottom row in Figure 7). First, fully two thirds of the neurons in M1 cortex are candidate oscillators (Figures 6D and 6E). Their intrinsic frequencies are low, essentially all below

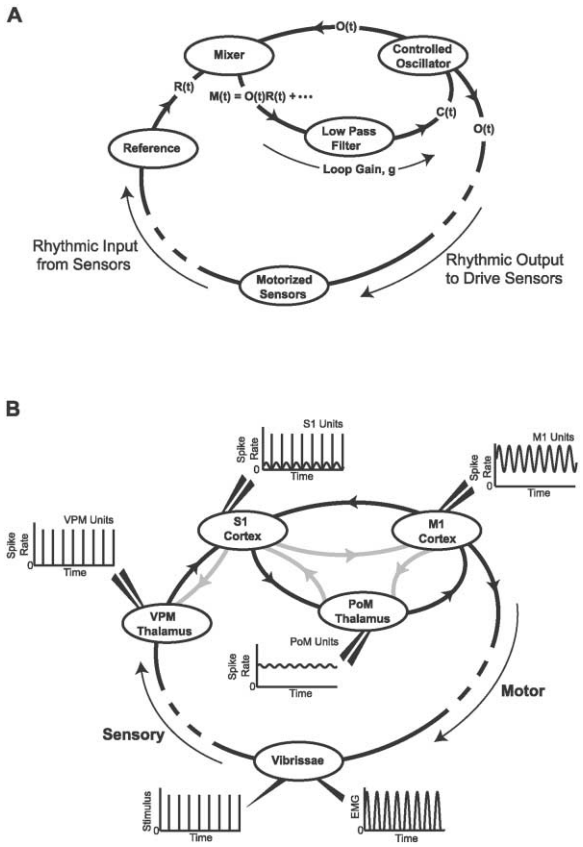

Figure 8. Model of the Analog Phase-Locked Loop for Adaptive Filtering and Summary of Thalamocortical Responses and Architecture Relevant to Adaptive Filtering in M1 Cortex

(A) A schematic of the analog phase-locked loop model is shown. The labels designate the signal pathways, with R(t) representing the input reference; O(t), the oscillator output, which is controlled by C(t); M(t), the mixer output, which contains the product of the "AC" parts of the two input signals; and g for the overall loop gain.

(B) The steady-state, stimulus-induced spiking outputs that are observed in different thalamocortical areas in response to periodic, punctate stimulation of the vibrissae are shown. The thick lines indicate known anatomical pathways. Lines in black, as opposed to gray, refer to pathways relevant to our model. The data for ventral posteriomedial (VPM) and posteriomedial (PoM) thalamus is abstracted from Ahissar and colleagues (Sosnik et al., 2001). We equate different thalamocortical areas with different parts of the loop: the VPM thalamus is equated with the input reference, vibrissa S1 cortex is equated with the mixer, vibrissa M1 cortex is equated with the oscillator, and PoM thalamus is equated with the low-pass filter and the propagation of the error signal.

10 Hz, which may prevent locking at a harmonic of the reference (e.g, a 5 Hz reference signal can lock to an oscillator with an intrinsic frequency of 10 Hz for sufficiently high values of loop gain, g) (Figure 8A and Equation 10). Second, the amplitude of the controlled oscillator is not expected to vary with frequency, consistent with our observations for units in M1 cortex (Figure 6A). Lastly, the phase difference between the oscillator output and that of the reference signal can be varied by a change in the loop gain or the intrinsic frequency of the controlled oscillator (Equation 10). This naturally leads to a uniform range of phases and is consistent with the range observed across different units in M1 cortex (Figure 6B). A final issue is that the output of an oscillator for rhythmic whisking must be gated between M1 cortices and the vibrissae. Catecholaminergic modulation of the threshold and sensitivity of vibrissa motoneurons provides one means for this control (McCall and Aghajanian, 1979).

Anatomical Basis for a Phase-Locked Loop

The sensorimotor loop of vibrissa-generated activity includes circuitry whose properties could support a transformation of vibrissa sensory information from S1 to M1 cortex by a phase-locked loop (Figure 8B). The vibrissa generate sensory signals that are faithfully transmitted through the lemniscal pathway to the ventral posterior medial (VPM) nucleus of the thalamus. This pathway is posited to provide a periodic reference signal of vibrissa contact to S1 cortex (R(t) in Figure 8A). In addition to direct sensory input, S1 cortex receives input from other cortical areas, notably vibrissa M1 cortex (Izraeli and Porter, 1995; Keller et al., 1996; Kim and Ebner, 1999). The electrical characteristics of this projection are uncharacterized but, by analogy with the input from S2 to S1 cortex, signals are likely to be delayed in time relative to those that originate via the lemniscal input. We speculate that some part of the long latency response in S1 cortex (Figure 3A) originates from feedback from M1 cortex (O(t) in Figure 8A). We further speculate that vibrissa S1 cortex acts to mix the incoming sensory and internal motor signals (M(t) in Figure 8A).

A second ascending sensory pathway from the whiskers through the trigeminal nuclei exists in parallel to the lemniscal pathway (i.e., the paralemniscal pathway). The paralemniscal pathway modulates the firing rate of cells in the medial division of the posterior thalamic nucleus. The neurons in the PoM nucleus show a shift in their latency such that the latency increases as a monotonic function of increasing stimulation rate (Sosnik et al., 2001). This does not occur in the lemniscal VPM nucleus (Sosnik et al., 2001). The dorsal part of PoM is reciprocally connected to all somatic-motor areas, including S1 and M1 cortices (Deschenes et al., 1998). Projections from cortical layer 6 in both cortical areas to PoM thalamus can modulate the firing rate of neurons in PoM thalamus. However, S1 cortex has additional projections from layer 5 cells that terminate on the proximal dendrites of neurons in PoM and generate an input that strongly drives neurons in PoM thalamus (Diamond et al., 1992; Veinante et al., 2000) (Figure 8B). In light of the shift in latency with increasing frequency and the strong drive from S1 cortex to PoM thalamus, we speculate that the PoM nucleus could act as a filter to adjust the frequency and gain of the PLL. Thus, the output of PoM thalamus serves as the feedback control signal (C(t) in Figure 8A).

The final component of the PLL circuit is the controlled oscillator. Our results suggest that vibrissa M1 cortex is a candidate structure for this role since neurons in M1 cortex have spontaneously rhythmic activity (Figures 6D and 6E) and, at least in part, are entrained to the fundamental stimulus frequency over a wide physiological range of frequencies (Figure 5). Further, they receive input from PoM thalamus (Deschenes et al., 1998).

In summary, we speculate that a subset of the thala-

mocortical circuitry comprising the S1 → PoM → M1 → S1 loop functions as a PLL to compute the fundamental frequency of a rhythmic, punctate stimulus. Starting with the sensory vibrissae, the lemniscal VPM nucleus provides the reference signal to S1 cortex. Vibrissa S1 cortex, in turn, is reciprocally connected with M1 cortex and PoM thalamus, which serve as the mixer, controlled oscillator, and phase detector, respectively (Figure 8B). Consistent with this hypothesis, work on the spread of epileptiform activity from M1 cortex shows that S1 and M1 cortices and PoM thalamus form a largely exclusive loop of neuronal activation (Bruehl et al., 1998). Finally, M1 cortex is in a position to modulate the discharge of motor neurons in the facial nerve nucleus that control the rate and amplitude of whisker movement as the rat explores the source and characteristics of behaviorally relevant stimuli within reach of the vibrissae.

Stimulus-Locked Modulation of the Spike Rate

A final issue concerns the degree to which the spike activity in M1 cortex is modulated by stimulation of the vibrissa in comparison with the degree of modulation in S1 cortex. Selection of the set of M1 cortical units in our data sample was essentially unbiased, as our criteria for selecting units in M1 cortex was only that the depth of the electrode lay near the layer 4/5 border and that there was a discernable level of background spike activity. Given these criteria, the average number of spikes per cycle that were locked to the stimulus is proportional to the amplitude of the sinusoidal modulation, $|c_1| = c_0 \times A_1$ (Equation 5), times the fraction of units that were phase locked to the stimulus and period of the cycle, denoted as T. Specifically, an average across our entire sample of sample units in vibrissa M1 cortex yields (Figures 6A and 6C) $\langle|c_1|\rangle \cdot T \equiv c_0 \cdot A_1 \cdot (75/197) \cdot T =$ (7.0 spikes/s) · (0.14) · (75/197) · (0.11 s/cycle) $\sim$ 0.04 spikes/cycle in response to periodic stimulation at 9 Hz. This number should be considered as a lower bound as we did not necessarily stimulate the optimal vibrissa for a given electrode penetration.

The apparently low modulation of the spike rate for units in M1 cortex (Figure 6A) must be considered in terms of the number of neurons whose outputs must be polled in order to achieve a reliable estimate of vibrissa position within a single cycle. To estimate this number, denoted n, we express the spike rate for the k-*th* unit by $r_k(t) = c_0 + |c_1| cos[\phi(t) + \phi_k]$, where $\phi(t) = 2\pi\nu_1 t$ and ϕ_k is the preferred phase. The number of units can be estimated in closed form under the assumption that: (1) the number of neurons is large (i.e., $n >> 1$), (2) the modulation depth is small (i.e., $c_0 >> |c_1|$), (3) individual units fire independently, and (4) the spike probabilities follow Poisson statistics. We define $\Delta\phi$ as the desired angular resolution, which we arbitrarily take to be $\Delta\phi = \pi/12$ radians, and use standard techniques (Dayan and Abbott 2002) and the observation that the ϕ_k are uniformly distributed (Figure 6B) to find $n = \pi \cdot (c_0/\langle|c_1|\rangle) \cdot (1/\langle|c_1|T\rangle) \cdot (2\pi/\Delta\phi)^2 \sim 4 \bullet 10^4$ neurons. This estimated number corresponds to a cortical volume of $\sim$0.5 mm^3, which is a small fraction of the $\sim$15 mm^3 total volume of M1 cortex (Figure 1A).

With regard to the modulation of the spike rate in S1 cortex, a calculation over all units in our data set shows that units in S1 cortex produced 0.5 spikes per cycle in response to stimulation, in agreement with the results of Simons (1978) for awake but paralyzed animals. On average, the short and long latency peaks contributed equally to the response of a given unit (Figure 3A). In estimating the extent of modulation, it is important to recall that the sampling of sensory responses here, as is likely in other work, was biased toward units with punctate responses and strong modulation by the stimulus. On the other hand, an unbiased sampling of the spiking output by units in S1 cortex suggests that, on average, these units produce 0.09 spikes per cycle as the rat whisks in air (Fee et al., 1997; O'Connor et al., 2002). The cycle-by-cycle modulation of the spiking output for units in S1 cortex is at most three times that for units in M1 cortex.

Concluding Remarks

Sensory signals are typically sharp in time and, thus, broad in their frequency composition. This property facilitates the accurate localization of objects in the sensory field. It applies equally well to both somatosensation, where signaling depends upon contact with an object, as to vision, where signaling depends on a transient change in contrast in the visual field. Active mechanical control of the sensor, be it the vibrissae or the eyes, is an essential aspect of scanning the environment and pursing targets. This control must be smooth and, thus, narrow-band filtered, as a means to avoid mechanical jerk and thus false signaling by the sensors. We suggest that the observed transformation from a punctate response in sensory cortex to a sinusoidal change in the motor cortex (Figure 3) represents a generic form of a control signal for rhythmic motor output.

Experimental Procedures

Animals and Implants

18 male adult Long Evan animals served as subjects. Four naïve animals were used for our mapping studies. The remaining 14 animals were gentled and habituated to head restraint as described (Bermejo et al., 1996; Cassella and Davis, 1987; Parry and McElligott, 1993; Sachdev et al., 2000). 10 to 14 days after the commencement of training, chambers were implanted over the vibrissa primary motor (M1) area of frontal cortex and the vibrissa primary sensory (S1) area of parietal cortex using procedures previously described (Sachdev et al., 2000). The interior of the chambers had a 7 mm bore. They were approximately centered over stereotaxic coordinates +2.5 mm anterior-posterior (A-P) and 1.5 mm medial-lateral (M-L) relative to the Bregma point for the chamber over M1 cortex and over stereotaxic coordinates −2 mm A-P and 5 mm M-L relative to the Bregma point for the chamber over S1 cortex. An approximately 4 mm diameter craniotomy was preformed in the middle of the chamber; the dura was left intact. The chambers were covered and the open cortex was cleaned and disinfected as required until measurements were performed. A post was mounted over the posterior aspect of the skull. In 7 of the animals, fine wires were implanted in the mystacial pad to record the electromyogram (EMG) of the muscles that move the vibrissae (Carvell et al., 1991).

Mapping of Vibrissa Movement

Rats were anesthetized with ketamine (50 mg per kg rat mass) and xylazine (15 mg per kg rat mass), held stereotaxically, and a craniotomy was made over frontal and the medial aspects of parietal cortex. We used the microstimulation paradigm of Donoghue and Wise (1982) to locate areas that led to motion of the vibrissae. A tungsten electrode (no. PI100305A1, Micro Probe, Inc., MD) was lowered at successive locations to stimulate cortex. The stimuli

consisted of a train of five unipolar 200 μs wide pulses, typically 10 to 60 μA in amplitude, that were delivered through the microelectrode at 2 ms intervals. The exact amplitude was chosen to be just above the threshold level for vibrissa movement but below a value that elicited nonspecific movement. Vibrissa movement was scored visually under microscopic observation.

Stimulus

Single vibrissae were stimulated with pulses of air, similarly to that in previous work (Ahissar et al., 2000; Fee et al., 1997; Sachdev et al., 2000). The puffs were 20 to 24 ms in duration (Figure 2A) and presented at a repetition rate that was systematically varied between 1 and 20 Hz. The stimulus pushed a vibrissa in the posteroventral direction. The exact onset time and duration of each pulse was recorded with a piezoelectric transducer (no. LTD0-028K, Measurement Specialties, Inc., NJ) whose output was sampled at a rate of 500 Hz. The amplitude of vibrissa deflection was measured with videography at a rate of 250 frames per s (Motion Scope, Redlake Inc., CA). The stimulation and video frame clocks were synchronized with a common logic pulse.

Recording

We recorded the responses in M1 and S1 cortices in nine animals. Our final data set consisted of 44 single units from M1 cortex and 23 single units from S1 cortex, each of which was measured at either a single frequency or a set of two to five different frequencies, for a total of 195 responses among motor cortical units and 53 among sensory units (31 concomitant with motor units). Recordings were judged to be from single units based on the absence of spikes near time shifts of zero in their autocorrelation (e.g., Figure 5A). The puff stimulus for each set of data was aligned to deflect only the vibrissa with the largest response in S1 cortex. Extracellular spike signals were recorded with high-impedance tungsten electrodes (2 to 10 MΩ at 1 kHz; WE3003 series, Frederick Haer, ME). Two to three independently controlled microdrives were attached to each chamber. Signals from the electrodes were amplified and band-pass filtered between 150 Hz and 9 kHz. Events that exceeded a threshold level that was nominally set at three times the background variation were sampled at 40 kHz and stored as 0.8 ms epochs with a commercial data acquisition system (MNAP, Plexon Inc., TX). The putative spike waveforms were analyzed offline and the quality of the data was judged from the autocorrelation. Typically, each electrode reported, at most, one single unit. In general, electrodes were lowered in both S1 and M1 cortices until unit activity was clearly discernable. For the case of units from S1 cortex, the final electrode positions were chosen to coincide with a unit that robustly spiked in response to deflection of a single vibrissa, as judged by an audio signal. We determined the primary vibrissa for each sensory unit by systematic mechanical deflection of individual vibrissae. For the case of M1 cortex, no units could be discerned on an audio monitor. The depth of each electrode was nominally kept between 500 and 1500 μm below the pia matter. Electromyogram signals were recorded with low-impedance electrodes that were formed from 50 μm tungsten wire (Fee et al., 1997). The signals were band-pass filtered between 200 Hz and 19 kHz, amplified, full-wave rectified, and low-pass filtered at 100 Hz (five-pole Butterworth) and sampled at 500 Hz. Spike acquisition and the EMG signals were synchronized by recording a common clock signal.

Histology

At the end of each recording session, one or more electrodes in each area were used to mark S1 and M1 cortices, respectively, with a pair of electrolytic lesions. We passed a constant current of 5 μA for 10 s at each location. Animals were then deeply anesthetized and perfused with physiological saline, followed by 4% (w/v) paraformaldehyde in physiological saline. The brains were extracted, cryoprotected in physiological saline with 30% (w/v) sucrose, blocked in the vicinity of M1 and S1 cortices, and sectioned on a sliding microtome at a thickness of 80 μm. Each section was stained for cytochrome-*c* oxidase activity (Wong-Riley, 1976). The lesions and associated histology were used to reconstruct recording tracks within M1 and S1 cortices.

Spectral Analysis

The output of a unit may be decomposed into two components under the condition of stationarity, i.e., that the firing statistics of a neuron remain constant over the time period of the measurement. The first component is a stimulus-induced response that is given by the trial-averaged spiking output (i.e., the peristimulus time histogram). The second component is the residual activity that is not locked to the stimulus and may also occur in the absence of stimulation. It is found by subtracting the average, stimulus-locked response from the data. This component is best described is terms of its statistical properties (e.g., the autocorrelation), or equivalently, the spectral power density. From the point of view of statistics, it is best to separate the data into its two components in the frequency domain (Percival and Walden, 1993). We thus calculated the spectrum of the stimulus-induced response in terms of spectral components at the fundamental and harmonic frequencies of the stimulus repetition rate. We used the multitaper methods of Thomson (1982) as a means to increase the number of degrees of freedom. We analyzed spike sequences of 100 s in duration, which had an intrinsic spectral resolution of 0.01 Hz, and chose to use final spectral resolutions of either 0.5 or 1.0 Hz. This led to 99 or 199 degrees of freedom, respectively. Confidence levels for a given spectral component were calculated by asymptotic methods (Jarvis and Mitra, 2001); we chose $p < 0.05$ as the level of significance. The spectrum of the residual response, along with its confidence interval, were similarly calculated. Following the above prescription, the full spectrum, denoted $\tilde{S}(\nu)$, is decomposed as

$$\tilde{S}(\nu) = \tilde{S}_{driven}(\nu) + \tilde{S}_{residual}(\nu). \quad (1)$$

The driven part of the spectral density, $\tilde{S}_{driven}(\nu)$, is expanded in terms of harmonics of the fundamental or drive frequency, ν_1, as

$$\tilde{S}_{driven}(\nu) = \sum_{n=1} |c_n|^2 \, \delta(\nu - n\nu_1), \quad (2)$$

where an expansion coefficient, c_n, is included only if it satisfies the 95% confidence interval. The coefficients are complex numbers and have units of spikes/s. The residual density, $\tilde{S}_{residual}(\nu)$, is defined as the smoothly varying remainder after the driven part is subtracted from the original density. The average rate or "DC" spectral component, c_0, is subtracted from the data prior to the spectral analysis.The spectral decomposition can also be used to define the linear transfer function. In the time domain, the transfer function is denoted T(t) and is given by

$$T(t) = c_0 + \sum_{n=1} |c_n| \, cos(2\pi \, n\nu_1 t + \phi_n) \text{ with } \phi_n = \tan^{-1}\left\{\frac{Im(c_n)}{Re(c_n)}\right\}, \quad (3)$$

where *Im*(z) and *Re*(z) refer to the imaginary part and real part of z, respectively. The function T(t) is statistically equivalent to the stimulus-triggered average.The benefit of spectral decomposition lies in the utility of an analytical form for the transfer function and in the ability to compute a confidence band for features of the transfer function (Figures 3A, 3E, and 5A–5D) or spectral density (Figures 3B–3D and 3F– 3I). This allows us to quantify features of the response. One feature is the fractional power in the driven response that is at the fundamental frequency, denoted $\delta S_{driven}(\nu_1)$, where

$$\delta S_{driven}(\nu_1) \equiv \frac{\int_0^\infty df |c_1|^2 \, \delta(\nu - \nu_1)}{\int_0^\infty df \sum_{n=1} |c_n|^2 \, \delta(\nu - n\nu_1)} = \frac{|c_1|^2}{\sum_{n=1} |c_n|^2}. \quad (4)$$

A second feature is the modulation amplitude, denoted A_1, and phase, ϕ_1, of the response at the fundamental frequency, where

$$A_1 = \frac{|c_1|}{c_0} \text{ and } \phi_1 = \tan^{-1}\left\{\frac{Im(c_1)}{Re(c_1)}\right\}, \quad (5)$$

so that the complete transfer function for the sinusoidal response of units in M1 cortex that are stimulated at frequency ν_1 can be

expressed as

$$T(t) = c_0\{1 + A_1 cos(2\pi\nu_1 t + \phi_1)\}. \quad (6)$$

Models of Linear and Adaptive Filters

The interpretation of our data on the nature of the unit response in M1 cortex depends on the form of response expected for different analog filters. In particular, we are interested in scenarios for which the sensory input, a train of pulses in the present case, is transformed into a sinusoid over a broad frequency range of frequencies.

Linear Filters

This is the case for which the input is convoluted with the kernel that parameterizes the filter; we denote the kernel by K(t). The most common kernel is a succession of single-pole or "RC" filters that are buffered from each other, as would occur with a synapse between cells. For low-pass filters, this kernel has the form

$$K(t) \propto \left(\frac{t}{\tau}\right)^{N-1} e^{-\frac{t}{\tau}}, \quad (7)$$

where τ is the filter time-constant, or equivalently $(2\pi\tau)^{-1}$ is the filter cut-off frequency, and N is the order of the filter. A second kernel that naturally arises in the study of nervous activity corresponds to dispersion by propagation along passive cables. The kernel has the form

$$K(t) \propto \sqrt{\frac{\tau}{t}}\, e^{-\left(\frac{t}{\tau} + \frac{X^2}{2}\frac{\tau}{t}\right)}, \quad (8)$$

where X is the distance that the signal propagates in units of electronic length.

Coupled Oscillators

This class consists of two groups of neurons that make reciprocal connections upon each other. One group of neurons, when oscillating on their own, produce rhythmic output at frequency ν_1. The second group, when oscillating on their own, produce rhythmic output at frequency ν_0. When the frequency difference is sufficiently small, the two populations may phase lock. In the limit that the connections are weak, the measured phase satisfies (Ermentrout and Kleinfeld, 2001; Kuramoto, 1984)

$$\phi = \sin^{-1}\left\{\frac{\pi(\nu_1 - \nu_0)}{j}\right\}, \quad (9)$$

where *j* is the pair-wise connection strength. Critically, locking will not occur if the connection strength is too small. We require

$$\pi(\nu_1 - \nu_0) < j\,.$$

Phase-Locked Loops

We consider a generic PLL that uses analog elements and sketch the essential condition for locking of the local oscillator to the reference (for a review, see Best, 1984). They consist of three main elements: a mixer, a controlled oscillator, and a low pass filter. This class of filters is characterized by response properties whose parameters, *e.g.*, cut-off frequency or bandwidth, can change in response to a change in the input.The input signals to the mixer consist of a reference pulse train and the output of the controlled oscillator, denoted R(t) and O(t), respectfully. The reference pulse train may be expressed as

$$R(t) = a_0 + \sum_{n=1} |a_n| cos(2\pi n\nu_1 + \phi_n)\,,$$

where the a_n are complex numbers that depend on the shape of the pulse, with magnitude and phase given by $|a_n|$ and $\phi_n = \tan^{-1}\{Im(a_n)/Re(a_n)\}$, respectively. The controlled oscillator has an output frequency of the form $\nu(t) = \nu_0 + f[C(t)]$, where C(t) is a control signal and $f(x)$ is a monotonically increasing function of x. Thus,

$$O(t) = b_0 + |b_1| cos\{2\pi[\nu_0 + f(E)]t + \phi\}\,,$$

where ϕ is the phase of the local oscillator. The output of the mixer, denoted M(t), is most simply taken as the product of the deviation of R(t) and O(t) from their mean values, i.e.,

$$M(t) = [R(t) - \bar{R}][O(t) - \bar{O}]\,.$$

This output is low-pass filtered (i.e., convoluted with a filter kernel K[t]) (see equations 7 or 8) and multiplied by an overall gain for the feedback loop, denoted g, so that the control signal to the oscillator, denoted C(t), is

$$C(t) = g\int_{-\infty}^{t} dt'\, M(t')K(t - t')\,.$$

The control signal will have a constant term, from the integral of the product R(t)O(t) in M(t), when the oscillator locks to the reference signal, as well as time varying terms. The time varying terms will be approach zero when the integration time of the filter is longer than the period of the stimulus.The phase of the local oscillator, ϕ, is found by a self-consistency argument in which the output of the oscillator satisfies $\nu_1 = \nu_0 + f(C)$ under lock. In this limit the control signal converges to

$$C(t) = g|a_n| sin(\Phi - \phi_n)\,,$$

where common prefactors were subsumed in the loop gain, so that self-consistency yields

$$n\nu_1 = \nu_0 + f\left(\frac{g|a_n|}{2\pi}\sin(\Phi - \phi_n)\right).$$

The measured phase thus satisfies

$$\Phi = \phi_n + \sin^{-1}\left(\frac{2\pi f^{-1}(n\nu_1 - \nu_0)}{g|a_n|}\right) \quad (10)$$

for locking at the n-*th* harmonic of ν_1. Note that locking will not occur if the loop gain is too small but that locking at harmonics will occur if the loop gain is too large Thus, for example, we require

$$\frac{2\pi f^{-1}(\nu_1 - \nu_0)}{|a_1|} < g < \frac{2\pi f^{-1}(2\nu_1 - \nu_0)}{|a_2|}\,,$$

to lock only at the fundamental frequency or repetition rate of the reference train. For a judicious choice of gain and reasonable models for the a_n, one can lock only to the fundamental frequency for pulse trains over a frequency range of a factor of two for arbitrary values of ν_0.

Acknowledgments

We thank Rune W. Berg and Suri Ventakachalam for assistance with the mapping studies; Gregory Champney for assistance with animals care and training; Ehud Ahissar, Charles D. Gilbert, Herbert Levine, Partha P. Mitra, and Haim Sompolinsky for useful conversations; and Beth Friedman for comments on an early version of the manuscript. This work was supported by grants from the NIH (MH59867 to D.K. and NS13031 to F.F.E.).

Received: October 18, 2001
Revised: April 9, 2002

References

Ahissar, E., Haidarliu, S., and Zackenhouse, M. (1997). Decoding temporally encoded sensory input by cortical oscillators and thalamic phase comparators. Proc. Natl. Acad. Sci. USA *94*, 11633–11638.

Ahissar, E., Sosnik, R., and Haidarliu, S. (2000). Transformation from temporal to rate coding in a somatosensory thalamocortical pathway. Nature *406*, 302–306.

Andersson, G. (1995). Cortico-cortical mediation of short-latency (lemniscal) sensory input to the motor cortex in deeply pentobarbitone anaesthetized cats. Acta Physiol. Scand. *153*, 381–392.

Armstrong-James, M., and Fox, K. (1987). Spatio-temporal convergence and divergence in the rat S1 "barrel" cortex. J. Comp. Neurol. *263*, 265–281.

Armstrong-James, M., and George, M.J. (1988). Bilateral receptive fields in rat Sm1 cortex. Exp. Brain Res. *70*, 155–165.

Armstrong-James, M., Fox, K., and Das-Gupta, A. (1992). Flow of

excitability within barrel cortex on striking a single vibrissa. J. Neurophysiol. *68*, 1345–1358.

Asanuma, H., Larsen, K., and Yumiya, H. (1980). Peripheral input pathways to the monkey motor cortex. Exp. Brain Res. *38*, 349–355.

Bermejo, R., Houben, D., and Zeigler, H.P. (1996). Conditioned whisking in the rat. Somatosens. Mot. Res. *13*, 225–234.

Best, R.E. (1984). Phase-Locked Loops: Theory, Design, and Applications (New York: McGraw-Hill).

Bruehl, C., Wagner, U., Huston, J.P., and Witte, O.W. (1998). Thalamocortical circuits causing remote hypometabolism during focal interictal epilepsy. Epilepsy Res. *32*, 379–387.

Carvell, G.E., and Simons, D.J. (1990). Biometric analyses of vibrissal tactile discrimination in the rat. J. Neurosci. *10*, 2638–2648.

Carvell, G.E., Simons, D.J., Lichtenstein, S.H., and Bryant, P. (1991). Electromyographic activity of mystacial pad musculature during whisking behavior in the rat. Somatosens. Mot. Res. *8*, 159–164.

Carvell, G.E., Miller, S.A., and Simons, D.J. (1996). The relationship of vibrissal motor cortex unit activity to whisking in the awake rat. Somatosens. Mot. Res. *13*, 115–127.

Cassella, J.V., and Davis, M. (1987). A technique to restrain awake rats for recording single-unit activity with glass micropipettes and conventional microdrives. J. Neurosci. Methods *19*, 105–113.

Chapin, J.K., and Lin, C.-S. (1984). Mapping the body representation in the SI cortex of anesthetized and awake rats. J. Comp. Neurol. *229*, 199–213.

Chapin, J.K., Waterhouse, B.D., and Woodward, D.J. (1981). Differences in cutaneous sensory response properties of single somatosensory cortical neurons in awake and halothane anesthetized rats. Brain Res. Bull. *6*, 63–70.

Chiaia, N.L., Rhoades, R.W., Fish, S.E., and Killackey, H.P. (1991). Thalamic processing of vibrissal information in the rat: II. morphological and functional properties of medial ventral posterior nucleus and posterior nucleus neurons. J. Comp. Neurol. *314*, 217–236.

Dayan, P., and Abbott, L.F. (2002). Theoretical Neuroscience: Computational and Mathematical Modeling of Neural Systems. (Cambridge, MA: MIT Press).

Deschenes, M., Veinante, P., and Zhang, Z.-W. (1998). The organization of corticothalamic pathways: reciprocity versus parity. Brain Res. Brain Res. Rev. *28*, 286–308.

Diamond, M.E., Budway, M.J., Armstrong-James, M., and Ebner, F.F. (1992). Somatic sensory responses in the rostral sector of the posterior group (POm) and in the ventral posterior medial nucleus (VPM) of the rat thalamus: dependence on the barrel field cortex. J. Comp. Neurol. *319*, 66–84.

Donoghue, J.P., and Sanes, J.N. (1988). Organization of adult motor cortex representation patterns following neonatal forelimb nerve injury in rats. J. Neurosci. *8*, 3221–3232.

Donoghue, J.P., and Wise, S.P. (1982). The motor cortex of the rat: cytoarchitecture and microstimulation mapping. J. Comp. Neurol. *212*, 76–88.

Donoghue, J.P., Suner, S., and Sanes, J.N. (1990). Dynamic organization of primary motor cortex output to target muscles in adult rats. II. rapid reorganization following nerve lesions. Exp. Brain Res. *79*, 492–503.

Ermentrout, G.B., and Kleinfeld, D. (2001). Traveling electrical waves in cortex: insights from phase dynamics and speculation on a computational role. Neuron *29*, 33–44.

Farkas, T., Kis, Z., Toldi, J., and Wolff, J.R. (1999). Activation of the primary motor cortex by somatosensory stimulation in adult rats is mediated mainly by associational connections from the somatosensory cortex. Neuroscience *90*, 353–361.

Fee, M.S., Mitra, P.P., and Kleinfeld, D. (1997). Central versus peripheral determinates of patterned spike activity in rat vibrissa cortex during whisking. J. Neurophysiol. *78*, 1144–1149.

Gioanni, Y., and Lamarche, M. (1985). A reappraisal of rat motor cortex organization by intracortical microstimulation. Brain Res. *344*, 49–61.

Herman, D., Kang, R., MacGillis, M., and Zarzecki, P. (1985). Responses of cat motor cortex neurons to cortico-cortical and somatosensory inputs. Exp. Brain Res. *57*, 598–604.

Hess, W.J. (1982). Algorithms and devices for pitch determination of speech signals. Phonetica *39*, 219–240.

Izraeli, R., and Porter, L.L. (1995). Vibrissal motor cortex in the rat: connections with the barrel field. Exp. Brain Res. *104*, 41–54.

Jacobs, K.M., and Donahue, J.P. (1994). Reshaping the cortical motor map by unmasking lateral intercortical connections. Science *251*, 944–947.

Jarvis, M.R., and Mitra, P.P. (2001). Sampling properties of the spectrum and coherency of sequences of action potentials. Neural Comput. *13*, 717–749.

Keller, A., Weintraub, D.N., and Miyashita, E. (1996). Tactile experience determines the organization of movement representations in rat motor cortex. Neuroreport *7*, 2373–2378.

Kim, U., and Ebner, F.F. (1999). Barrels and septa: separate circuits in rat barrels field cortex. J. Comp. Neurol. *14*, 489–505.

Kleinfeld, D., and Delaney, K.R. (1996). Distributed representation of vibrissa movement in the upper layers of somatosensory cortex revealed with voltage sensitive dyes. J. Comp. Neurol. *375*, 89–108. Erratum: J. Comp. Neurol. *378*, 1997.

Kleinfeld, D., Berg, R.W., and O'Connor, S.M. (1999). Anatomical loops and their relation to electrical dynamics in relation to whisking by rat. Somatosens. Mot. Res. *16*, 69–88.

Kuramoto, Y. (1984). Chemical Oscillations, Waves and Turbulence (New York: Springer Verlag).

Mays, L.E., and Sparks, D.L. (1980). Saccades are spatially, not retinocentrically, coded. Science *208*, 1163–1165.

McCall, R.B., and Aghajanian, G.K. (1979). Serotonergic facilitation of facial motoneuron excitation. Brain Res. *169*, 11–27.

Miyashita, E., Keller, A., and Asanuma, H. (1994). Input-output organization of the rat vibrissal motor cortex. Exp. Brain Res. *99*, 223–232.

Neafsey, E.J., Bold, E.L., Haas, G., Hurley-Gius, K.M., Quirk, G., Sievert, C.F., and Terreberry, R.R. (1986). The organization of the rat motor cortex: a microstimulation mapping study. Brain Res. Brain Res. Rev. *11*, 77–96.

Nicolelis, M.A.L., Baccala, L.A., Lin, R.C.S., and Chapin, J.K. (1995). Sensorimotor encoding by synchronous neural ensemble activity at multiple levels of the somatosensory system. Science *268*, 1353–1358.

O'Connor, S.M., Berg, R.W., and Kleinfeld, D. (2002). Coherent electrical activity between vibrissa sensory areas of cerebellum and neocortex is enhanced during free whisking. J. Neurophysiol. *87*, 2137–2148.

Parry, T.J., and McElligott, J.G. (1993). A method for restraining awake rats using head immobilization. Physiol. Behav. *53*, 1011–1015.

Percival, D.B., and Walden, A.T. (1993). Spectral Analysis for Physical Applications: Multitaper and Conventional Univariate Techniques (Cambridge: Cambridge University Press).

Pierce, J.R. (1991). Periodicity and pitch perception. J. Acoust. Soc. Am. *90*, 1889–1893.

Sachdev, R.N., Sellien, H., and Ebner, F.F. (2000). Direct inhibition evoked by whisker stimulation in somatic sensory (S1) barrel field cortex of the awake rat. J. Neurophysiol. *84*, 1497–1504.

Sanderson, K.J., Welker, W., and Shambes, G.M. (1984). Reevaluation of motor cortex and of sensorimotor overlap in cerebral cortex of albino rats. Brain Res. *292*, 251–260.

Sharp, F.R., and Evans, K. (1982). Regional (14C) 2-deoxyglucose uptake during vibrissae movements evoked by rat motor cortex stimulation. J. Comp. Neurol. *208*, 255–287.

Simons, D.J. (1978). Response properties of vibrissal units in rat S1 somatosensory neocortex. J. Neurophysiol. *41*, 798–820.

Simons, D.J. (1983). Multi-whisker stimulation and its effects on vibrissa units in rat SmI barrel cortex. Brain Res. *276*, 178–182.

Simons, D.J. (1985). Temporal and spatial integration in the rat SI vibrissa cortex. J. Neurophysiol. *54*, 615–635.

Sompolinsky, H., Golomb, D., and Kleinfeld, D. (1990). Global processing of visual stimuli in a neural network of coupled oscillators. Proc. Natl. Acad. Sci. USA *87*, 7200–7204.

Sosnik, R., Haidarliu, S., and Ahissar, E. (2001). Temporal frequency of whisker movement. I. representations in brain stem and thalamus. J. Neurophysiol. *86*, 339–353.

Swadlow, H. A. (1994). Efferent neurons and suspected interneurons in motor cortex of the awake rabbit: axonal properties, sensory receptive fields, and subthreshold synaptic inputs. J. Neurophysiol. *71*, 437–453.

Thomson, D.J. (1982). Spectral estimation and harmonic analysis. Proceedings of the IEEE *70*, 1055–1096.

Veinante, P., Lavallee, P., and Deschenes, M. (2000). Corticothalamic projections from layer 5 of the vibrissal barrel cortex in the rat. J. Comp. Neurol. *424*, 197–204.

Weiss, D.S., and Keller, A. (1994). Specific patterns of intrinsic connections between representation zones in the rat motor cortex. Cereb. Cortex *4*, 205–214.

Welker, C. (1971). Microelectrode delineation of fine grain somatotopic neocortex of the rat. Brain Res. *26*, 259–275.

Wong-Riley, M.T.T. (1976). Endogenous peroxidatic activity in brain stem neurons as demonstrated by their staining with diaminobenzidine in normal squirrel monkeys. Brain Res. *108*, 257–277.

Woolsey, T.A., and Van der Loos, H. (1970). The structural organization of layer IV in the somatosensory region (SI) of mouse cerebral cortex. Brain Res. *17*, 205–242.